RESEARCH ARTICLE

A Low-Loss and Full-360° Reflection-Type Phase Shifter for WLAN Wireless Backhaul Applications

WENJIAN MA [ID] [1], **PEI ZOU** [2], **LIBING BAI** [ID] [1], (Member, IEEE), **AND KAI CHEN** [ID] [1], (Member, IEEE)
[1] School of Automation Engineering, University of Electronic Science and Technology of China, Chengdu 611731, China
[2] Tenth Institute of China Electronics Technology Group Corporation, Chengdu 610036, China

Corresponding author: Libing Bai (libing.bai@uestc.edu.cn)

ABSTRACT This paper presents a reflective-type phase shifter (RTPS) capable of a full 360° phase shift range with low-loss and compact for 5.47–5.85-GHz WLAN wireless backhaul. Intuitive and concise analyses of common reflective loads, including single-element single-tunable (SEST), dual-element single-tunable (DEST), and three-element single-tunable (TEST), are analyzed, elaborating their limitations. The four-element dual-tunable (FEDT) load technique is proposed to increase the phase shift range. In addition, the influence factors of phase shift step and insertion loss (IL) are comprehensively discussed. Measurement results show that the proposed RTPS provides a phase shift range greater than 360°, a phase shift step less than 15°, and an IL less than 2.3-dB in the entire frequency band. Meanwhile, the size of this RTPS is only 9.5×8.2 mm^2. Compared to other RTPS, this design has the advantages of low IL, compact size, wide band, high precision, and easy control.

INDEX TERMS Digital tunable capacitor (DTC), reflective-type phase shifter (RTPS), WLAN wireless backhaul.

I. INTRODUCTION

Small cell base stations with small size and flexible deployment have become the mainstream for increasing cell density in 5G wireless communication. Compared to the point-to-point link of optical fiber and microwave, the 5 GHz WLAN wireless backhaul combines the advantages of low cost, wide band, and non-line-of-sight (NLOS) [1], [2]. However, interference such as Access Point (AP) is the biggest challenge for WLAN wireless backhaul, the first step to suppress interference is beamforming with multiple phase shift arrays to generate a large null depth [3], [4]. The application scenario is illustrated in Fig. 1(a).

As shown in Fig. 1(b), the WLAN wireless backhaul device with 8 RF paths, and every path has 7 phase shift channels can provide high channel capacity and interference suppression.

The associate editor coordinating the review of this manuscript and approving it for publication was Mohammed Bait-Suwailam [ID].
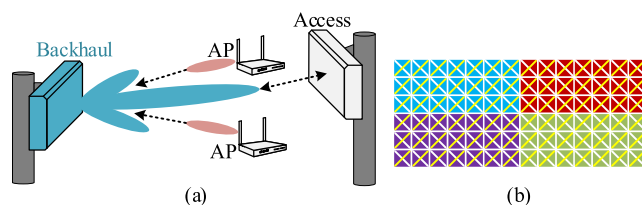
FIGURE 1. WLAN wireless backhaul applications. (a) Interference suppression scenario. (b) 4T8R vertical and horizontal dual-polarized antenna array.

To achieve the above performance, Besides the wide phase shift range, the phase shifter should also provide low insertion loss (IL), small phase shift step, and compact size [5].

Reflective-type phase shifter (RTPS) has the advantages of low IL, compact size, high linearity, wide band, low power consumption, and continuous adjustability [6], which has become an excellent solution and research focus for

Massive MIMO and wireless backhaul systems. In [7] and [8], varactor diodes were used as tuning elements of RTPS, which require high control voltage to reduce IL, the complex peripheral circuits and high power consumption caused by high voltage control are the fatal flaws to achieve large-scale phase-shifting arrays. To simplify the complexity of control circuits, the digital tuning elements were realized by RF microelectromechanical systems (MEMS) devices [9], which have the advantages of low power consumption, but the large switching time increases the convergence time of the anti-jamming algorithm for multi-beam forming, and the 5-bit RF MEMS capacitors produce larger phase shift step. Additionally, the load topology with series and parallel forms were analyzed in [10], due to the limitation of the number of tuning elements in the load topology, a phase shift range of 270° just can be reached. Alternatively, RTPS with a dual-branch switching network found in [11] and a two-stage cascade structure found in [12] could achieve a 360° phase shift range, but the dual-branch and cascading result in an increase in IL and size.

To address these challenges and meet the demanding performance requirements of the WLAN wireless backhaul system, we propose a 5.47-5.85 GHz RTPS using the four-element dual-tunable (FEDT) load technique to achieve a full 360° phase shift range, low IL, small phase shift step, and compact size simultaneously. Theoretically, the performance of popular reflective loads is carried out by a simple geometric method. Furthermore, a systematic design methodology of the RTPS using FEDT load topology is developed, and the Silicon-On-Insulator (SOI) digital tunable capacitor (DTC) is adopted to derive the methods of reducing the phase shift step and IL.

II. PHASE SHIFTER ANALYSIS

A. REFLECTIVE LOAD TOPOLOGY

Fig. 2(a) presents a typical RTPS topology that consists of a 90° hybrid coupler and two identical tunable passive reflective loads [13], [14]. Considering the 3 dB 90° coupler as ideal, and the two loads remain consistent ($Z_{L1} = Z_{L2} = Z_L$), the output phase shift $\angle\Phi$ and IL of the RTPS can be derived as

$$\angle\Phi = \angle\Gamma_L + 90°, IL = -20\log(|\Gamma_L|) \quad (1)$$

where Γ_L is the reflection coefficient of the reflective loads. For ideal lossless loads, $Z_L = jX_L$, $|\Gamma_L| = 1$. Simultaneously, the lossless loads and phase shift range satisfy

$$(jX_L - Z_0)/(jX_L + Z_0) = e^{j\angle\Gamma_L} = e^{j\varphi} \quad (2)$$

then the phase shift φ can be expressed as

$$\cot\varphi = \frac{X_L^2 - Z_0^2}{2X_L Z_0} = \frac{x^2 - 1}{2x} \Rightarrow \varphi = \pi - 2\operatorname{atan}(x) \quad (3)$$

where $x = X_L/Z_0$ is the normalized impedance.

For $x \in [-20, 20]$, the phase change with load normalized impedance as shown in Fig. 2(b), suggests that we can get a 360° phase shift range by changing the load impedance.
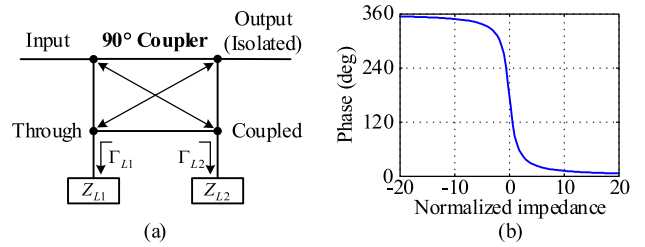

FIGURE 2. Phase-shifting principle of RTPS. (a) Typical RTPS topology, and (b) phase changes with load impedance.

The design of load topology is very important for the phase shift range index of RTPS, there are multiple methods to adjust the load impedance [15]. Next, we will present several reported reflective load topologies and analyze their load impedance tuning range more concisely and intuitively.

The simplest reflective load in an RTPS is single-element single-tunable (SEST), which includes a single-tunable inductor or single-tunable capacitor [16]. Fig. 3(a) shows a single tunable inductor load and its theoretical phase tunable range $\varphi \in (0°, 180°)$ with load impedance $Z_L = j\omega L$. Similarly, Fig. 3(b) shows a single tunable capacitor load and its theoretical phase tunable range $\varphi \in (180°, 360°)$ with load impedance $Z_L = -j/\omega C$. The maximum theoretical phase shift range of SETA is close to 180°. However, due to the limitation of the tuning range of the adjustable element, the actual phase shift range will be much lower than the theoretical value.

To further extend the phase shift range, dual-element single-tunable (DEST) reflective loads are used in RTPS [10], which include series L-C loads [Fig. 3(c)] or parallel L-C loads [Fig. 3(d)]. The load impedance Z_L of series L-C is $j[(\omega^2 LC - 1)/(\omega C)]$ and its theoretical phase tunable range $\varphi \in (360°, 0°)$. When $\omega^2 LC = 1$, that is $x_L = x_C$, where $x_L = \omega L$, $x_C = 1/(\omega C)$, and the series L-C loads generate a series resonance point where $\varphi = 180°$. Correspondingly, the load impedance Z_L of parallel L-C is $j\omega L/(1 - \omega^2 LC)$, and its theoretical phase tunable range $\varphi \in (+180°, -180°)$. When $\omega^2 LC = 1$, that is $x_L = x_C$, the parallel L-C loads generate a parallel resonance point where $\varphi = 0°$. The tunable element C can be tuned from $C_{\min}$ to $C_{\max}$, the achievable minimum and maximum capacitance. Unfortunately, the phase shift of DEST reflective loads remains <360° because the $C_{\max}/C_{\min}$ can never be ∞ in practice. But compared with SEST, DEST can achieve a larger phase shift range [17].

To further increase the phase shift range, three-element single-tunable (TEST) has been considered. As shown in Fig. 4, TEST reflective loads still have only one tunable element, which can be seen as an extension of DEST. Taking Fig. 4(a) as an example, the load impedance Z_L can be expressed as

$$Z_L = j\frac{\omega^2 CL - 1}{\omega(C + C_1 - \omega^2 LCC_1)} \quad (4)$$

It can be found that TEST reflective loads only cover one series resonance point and one parallel resonance point, that
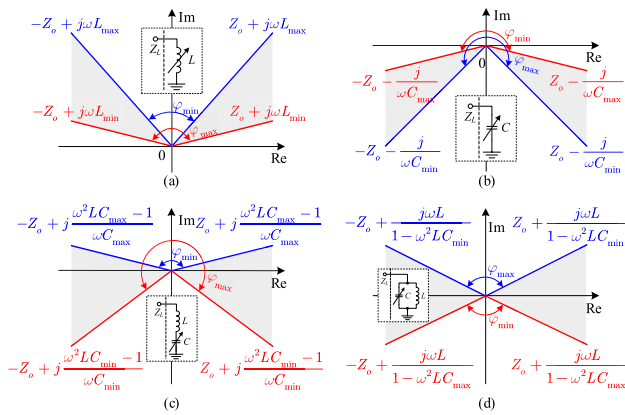
FIGURE 3. (a) The theoretical phase shift range for a single tunable capacitor load, (b) the theoretical phase shift range for a single tunable inductor load, (c) the theoretical phase shift range for series L-C loads by tuning C, and (d) the theoretical phase shift range for parallel L-C loads by tuning C.

is infinite point, which still cannot achieve 360° phase shift range. However, since the TEST reflective loads cover two resonance points, under the same C_{max}/C_{min} radio, a larger phase shift range can be obtained than DEST reflective loads.
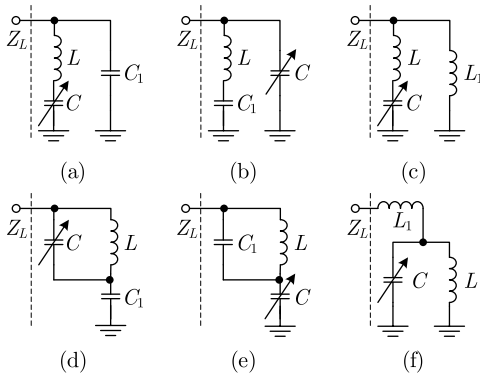
FIGURE 4. Reflective loads of three-element single-tunable (TEST).

In summary, the phase shift range of a single tunable element load topology is less than 360°, which is limited by the number and tuning range of the tunable element. The RTPS that uses high-order four-elements dual-tunable (FEDT) as the load is illustrated in Fig. 5(a), which is an excellent solution to achieve a 360° phase shift range.
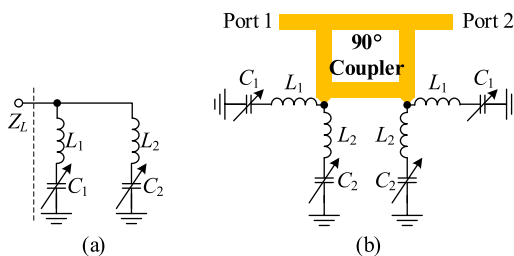
FIGURE 5. Reflective loads of four-element dual-tunable (FEDT). (a) Load topology, and (b) phase shift topology.

The phase shift topology of FEDT is shown in Fig. 5(b), and the load impedance Z_L is given by

$$Z_L = \frac{Z_1 \times Z_2}{Z_1 + Z_2} = j\frac{(X_{L1} - X_{C1}) \times (X_{L2} - X_{C2})}{(X_{L1} - X_{C1}) + (X_{L2} - X_{C2})} \quad (5)$$

Further, the normalized impedance of Z_L can be expressed as

$$x = \frac{X_L}{Z_0} = \frac{(x_{L1} - x_{C1}) \times (x_{L2} - x_{C2})}{(x_{L1} - x_{C1}) + (x_{L2} - x_{C2})} = \frac{x_n}{x_d} = \cot\frac{\varphi}{2} \quad (6)$$

where

$$x_n = (x_{L1} - x_{C1}) \times (x_{L2} - x_{C2})$$
$$x_d = (x_{L1} - x_{C1}) + (x_{L2} - x_{C2}) \quad (7)$$

Meanwhile, set $x_{Cmin} \geq x_{L1} \geq x_{L2} \geq x_{Cmax}$, as shown in Fig. 6(a). By adjusting C_1 and C_2 in sequence, the phase change passes through the open and short points on the Smith chart, that is, the phase is changed from $+180°$ to $-180°$, and a 360° full-span phase shift range can be achieved.
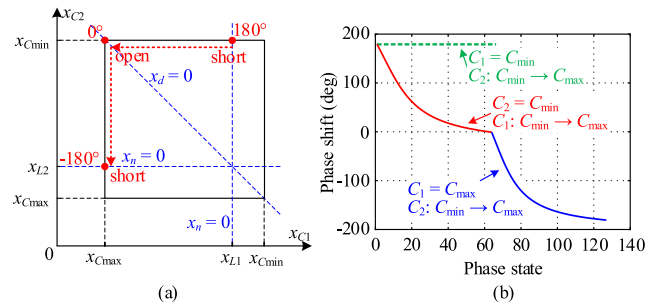
FIGURE 6. 360° phase shift method. (a) Phase shift path, and (b) phase changes with state.

To ensure a full 360° phase shift range, L_1 and L_2 are designed to generate series resonance with C_{min} and C_{max}

$$L_1 = 1/\left(\omega_0^2 C_{min}\right), L_2 = 1/\left(\omega_0^2 C_{max}\right) \quad (8)$$

where ω_0 is the center frequency of the operating band. When the tunable capacitor is realized by DTC, which has 6-bit resolution and 64 capacitance states. As shown in Fig. 6(b), the 360º phase shift range can be obtained by twice adjustments of C_1 and C_2:

*Step* 1: Fix $C_2 = C_{min}$, and adjust C_1 from C_{min} to C_{max}, the phase changes from $+180º$ to $0º$.

Step 2: Fix $C_1 = C_{max}$, and adjust C_2 from C_{min} to C_{max}, the phase changes from $0º$ to $-180º$.

If we fix $C_1 = C_{min}$ and adjust C_2 from C_{min} to C_{max}, the phase will be fixed at $180º$. Consequently, we must follow a certain order to adjust the capacitance of DTCs.

B. PHASE SHIFT STEP

The phase shift step [Fig. 7(a)] can be obtained by differentiating the phase shift curve in Fig. 6 (b). In addition to increasing the bit width of DTCs, as depicted in Fig. 7(b), the phase shift step can also be optimized by reducing C_{max}, adjusting L_1 and L_2 to obtain optimal impedance matching simultaneously. As shown in Fig. 7(c), under the condition of

constant C_{min}, the smaller of C_{max}/C_{min} results in a smaller phase shift step. In terms of inductance lines, compared with perfect matching, smaller or larger inductance lines will lead to the increasing of phase shift step as illustrated in Fig. 7(d). Since the inductance lines are not adjustable generally, it is necessary to ensure that the inductance lines are well matched with C_{min} and C_{max} at the center frequency to obtain good performance for wide bands.
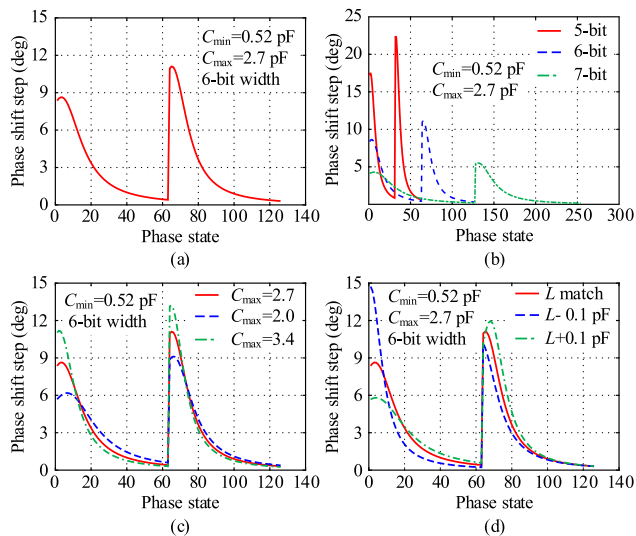
FIGURE 7. Influencing factors of phase shift step. (a) The phase shift step is obtained by differentiating the 360° phase shift curve, (b) the influence of DTC bits, (c) the influence of DTC C_{max}, and (d) the influence of inductance lines.

C. INSERTION LOSS

Because of the circuits are non-ideal, the performance of 90° coupler (IL, isolation, etc.) and load topology (ESR, matching, etc.) cause the IL to RTPS. As shown in Fig 8(a), the phase shift path on the Smith chart does not move along the lossless ring. Particularly, the ESR of load is the key to affecting the IL of RTPS.
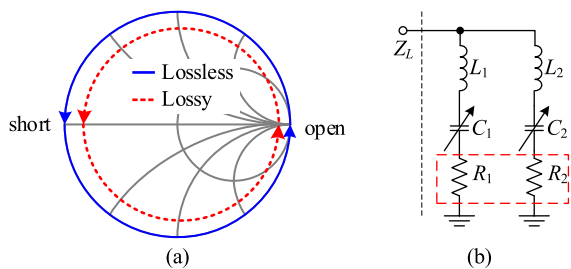
FIGURE 8. Load topology and phase shift path considering ESR. (a) The phase shift path of lossless and lossy topology, and (b) the ESR of load topology.

As shown in Fig 8(b), when $Z_{L1} = Z_{C1}$ and $Z_{L2} = Z_{C2}$, the load topology has a series resonant point, according to formula (8), the $C_1 = C_{min}$ and $C_2 = C_{max}$. Therefore, the

impedance Z_L of the load topology can be expressed as

$$Z_L = \frac{R_1 R_2}{R_1 + R_2} \quad (9)$$

Based on formula (1), the IL is smallest at the series resonance point, but when $C_1 = C_{min}$, the phase of RTPS is nonadjustable.

When $Z_{L1+C1} = -Z_{L2+C2}$, the load topology has a parallel resonance point, the relationship of C_1 and C_2 can be given by

$$\frac{1}{C_1} + \frac{1}{C_2} = \frac{1}{C_{min}} + \frac{1}{C_{max}} \quad (10)$$

Let $C_1 = C_{max}$ and $C_2 = C_{min}$, the load Z_L can be expressed as

$$Z_L = \frac{\left(\frac{C_{max} - C_{min}}{\omega C_{min} C_{max}}\right)^2 + \frac{j(R_2 - R_1)(C_{max} - C_{min})}{\omega C_{min} C_{max}} + R_1 R_2}{R_1 + R_2} \quad (11)$$

From (11), the bigger the value of C_{max}/C_{min}, the closer $|Z_L|$ gets to positive infinity, which effectively increases the Q of the parallel resonance and results in a smaller IL.

Compared with RF MEMS, RF SOI has higher reliability and faster RF path switching time, this paper adopts 6-bit RF SOI DTC as the tunable elements. As shown in Fig.9(a), the tuning range of this DTC is about 0.52-2.70 pF at 5.66 GHz, which has 64 states with a step of 34.6 fF. The ESR of the DTC is about 0.93-0.33 Ω, which decreases with the increase of capacitance. Substituting the capacitance and ESR parameter of RF SOI DTC into formula (2), the 2D color plot of $|\Gamma_L|$ is obtained, which is presented in Fig. 9(b). According to the configuration order of C_1 and C_2, two IL curves are depicted in Fig. 10(a). Although the blue dashed line has better IL performance and has a series resonance point with the smallest IL, combined with the previous analysis of phase shift range, the phase cannot be changed in this traversal method. Hence, we can only adjust C_1 first, then C_2, to get the IL curve of the red solid line.
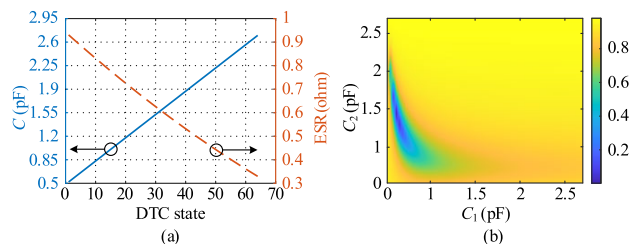
FIGURE 9. (a) Tuning range and ESR of DTC. (b) The 2D color plot of $|\Gamma_L|$ changes with C_1 and C_2.

Furthermore, except for the ESR of DTC [see Fig. 10(b)], the C_{max} and the impedance matching of inductance lines also have a great effect on IL. As depicted in Fig. 10(c) and (d), to get a smaller phase shift step, C_{max}/C_{min} should be small, but the smaller the C_{max}/C_{min}, the larger the IL. Therefore, we should make a compromise between the phase shift step and IL to choose the optimal capacitance range.

TABLE 1. Comparison between the proposed design and previous works.

Ref.	Freq. (GHz)	Substrate	Phase shift range (°)	Phase shift step (°)	IL (dB)	*FoM (°/dB)	Size (mm²)	Tuning mode
[7]	1.9-2.1	N/A	>360	N/A	<5.8	>62	56×30	Voltage (0-5 V)
[8]	5.6-6.0	Roger 6002	>270	N/A	<3.5	>77	24×21	Voltage (0-20 V)
[9]	1.9-2.1	Rogers 4003	>325	<25	<3.3	>98	28×30	Digital (5-bit)
[10]	2.3-2.4	FR4	>270	N/A	<4.5	>60	20×10	Voltage (0-20 V)
[11]	2.35-2.55	Rogers 6010	>360	N/A	<7.5	>48	20×23	Voltage (0-9 V)
[12]	3.45-3.55	FR4	>345	N/A	<11.2	>30	70×60	Voltage (0-5 V)
This work	5.47-5.85	Rogers 4350	>360	<15	<2.3	>156	9.5×8.2	Digital (6-bit)

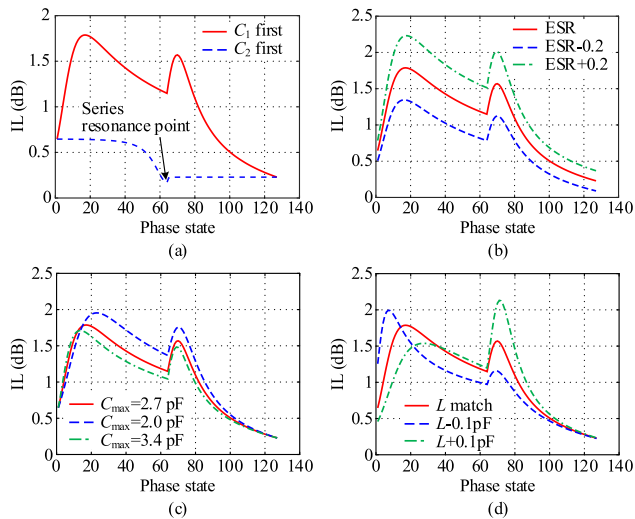*FoM = maximum phase shift (in degrees)/maximum insertion loss (in dB)

FIGURE 10. Influencing factors of IL. (a) Traversal priority of two DTCs, (b) the influence of ESR, (c) the influence of DTC range, and (d) the influence of inductance lines.
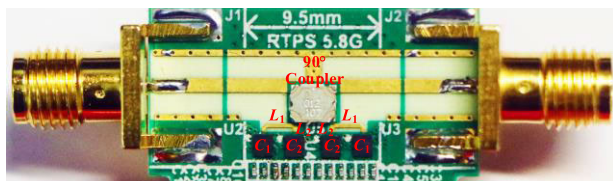

FIGURE 11. Design diagram of RTPS.

FIGURE 12. Measured phase shift versus frequency. (a) All phase states, and (b) select phase state to achieve about 11.25° equally spaced phase shift step.

FIGURE 13. The measured and simulated data of RTPS. (a) The measured data of phase change. (b) The measured data of phase step. (c) The measured data of IL. (d) The measured and simulated results of phase shift range.

III. DESIGN AND MEASUREMENT RESULTS

The phase shifter is built on a Rogers 4350 substrate with $h = 20$ mil, $\varepsilon_r = 3.48$, and $\tan\delta = 0.0037$. Moreover, the inductance lines are realized by microstrip lines that $L_1 = 1.52$ nH and $L_2 = 0.29$ nH at 5.66 GHz. Advanced Design System (ADS) is used for optimization and simulation, to ensure RTPS can reach a 360° phase shift range in the full frequency band of 5.47- 5.85 GHz. The final RTPS is shown in Fig. 11.

Fig. 12(a) demonstrates the measured phase shift range for the entire frequency band by twice adjustments of C_1 and C_2. Due to a large number of states, we present test data at high, medium, and low frequency points in more detail in Fig. 13. The measured results of the phase shift change, phase shift step, and IL of RTPS are shown in
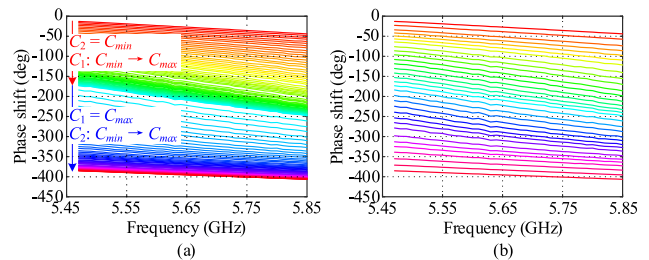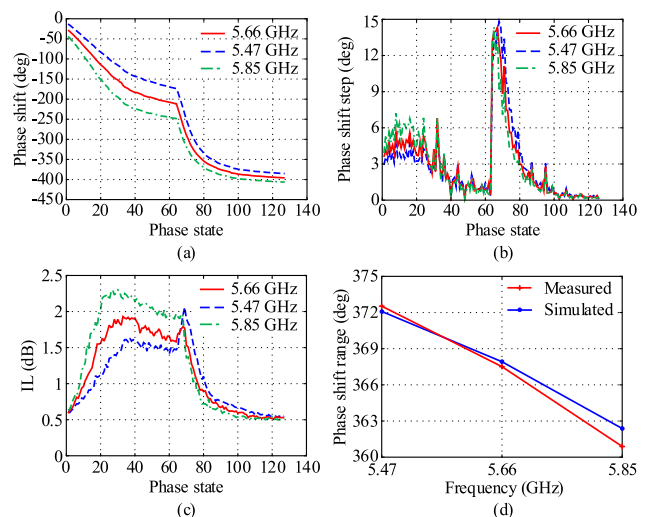
Fig. 13(a), (b) and (c) respectively. At the edge frequency that 5.47 GHz and 5.85 GHz, IL and phase-shift step both display dispersion phenomenon, which is consistent with the theoretical analysis of the impedance matching of inductance lines. In the entire frequency band, the phase shift step is less than 15°, and the IL is less than 2.3 dB. As shown in Fig. 13(d), there is excellent agreement between measurements and simulations in the phase shift range. Combining the results of phase shift range and phase shift step, a 360° high-precision phase shifter with about 5-bit equally spaced phase shift step (about 11.25°) can be realized [see Fig. 12(b)].

Table 1 shows the comparison of this work and RTPSs found in the literature. Obviously, this work has the advantages of large bandwidth, large phase shift range, small phase shift step, low IL, and high integration simultaneously.

IV. CONCLUSION

This paper presents a full 360° RTPS with low IL and high integration using the FEDT load technique. The major factors that affect phase shift range, phase shift step, and IL have been analyzed by a simple geometric method. Measurement results show that the proposed phase shifter has a 360° phase shift range with 2.3 dB IL, 11.25° phase shift step, and only 9.5×8.2 mm^2 at the WLAN frequency band from 5.47 to 5.85 GHz, which can meet the demands of the WLAN wireless backhaul applications completely.

REFERENCES

[1] C. Saha, M. Afshang, and H. S. Dhillon, "Bandwidth partitioning and downlink analysis in millimeter wave integrated access and backhaul for 5G," *IEEE Trans. Wireless Commun.*, vol. 17, no. 12, pp. 8195–8210, Dec. 2018.

[2] M. Á. Vázquez, L. Blanco, and A. I. Pérez-Neira, "Hybrid analog–digital transmit beamforming for spectrum sharing backhaul networks," *IEEE Trans. Signal Process.*, vol. 66, no. 9, pp. 2273–2285, May 2018.

[3] T. LeAnh, N. H. Tran, D. T. Ngo, Z. Han, and C. S. Hong, "Orchestrating resource management in LTE-unlicensed systems with backhaul link constraints," *IEEE Trans. Wireless Commun.*, vol. 18, no. 2, pp. 1360–1375, Feb. 2019.

[4] C.-H. Chang, J.-Y. Chen, C.-T. Shen, M.-J. Tsai, and T.-S. Tai, "Reflection-type phase shifter integrated with tunable power attenuation mechanism for sub-6 GHz wireless applications," *IEEE Access*, vol. 10, pp. 115532–115540, 2022.

[5] Q. Wu and R. Zhang, "Beamforming optimization for wireless network aided by intelligent reflecting surface with discrete phase shifts," *IEEE Trans. Commun.*, vol. 68, no. 3, pp. 1838–1851, Mar. 2020.

[6] A. Chakraborty and B. Gupta, "Paradigm phase shift: RF MEMS phase shifters: An overview," *IEEE Microw. Mag.*, vol. 18, no. 1, pp. 22–41, Jan. 2017.

[7] C.-S. Lin, S.-F. Chang, and W.-C. Hsiao, "A full-360° reflection-type phase shifter with constant insertion loss," *IEEE Microw. Wireless Compon. Lett.*, vol. 18, no. 2, pp. 106–108, Feb. 2008.

[8] M. A. El-Tanani and G. M. Rebeiz, "C-band low-loss phase shifter >360° for WLAN applications," in *Proc. Eur. Microw.*, Oct. 2007, pp. 1503–1506.

[9] O. D. Gurbuz and G. M. Rebeiz, "A 1.6–2.3-GHz RF MEMS reconfigurable quadrature coupler and its application to a 360° reflective-type phase shifter," *IEEE Trans. Microw. Theory Techn.*, vol. 63, no. 2, pp. 414–421, Feb. 2015.

[10] V. Kirillov, D. Kozlov, and S. Bulja, "Series vs parallel reflection-type phase shifters," *IEEE Access*, vol. 8, pp. 189276–189286, 2020.

[11] C.-E. Guan and H. Kanaya, "360° phase shifter design using dual-branch switching network," *IEEE Microw. Wireless Compon. Lett.*, vol. 28, no. 8, pp. 675–677, Aug. 2018.

[12] Y. Yin, F. Wu, Y. Chen, J. Zhou, and J. Zhai, "Design of a cascaded full 360° reflection-type phase shifter with 90° hybrid coupler," in *IEEE MTT-S Int. Microw. Symp. Dig.*, May 2018, pp. 1–3.

[13] R. Garg and A. S. Natarajan, "A 28-GHz low-power phased-array receiver front-end with 360° RTPS phase shift range," *IEEE Trans. Microw. Theory Techn.*, vol. 65, no. 11, pp. 4703–4714, Nov. 2017.

[14] A. Basaligheh, P. Saffari, S. Rasti Boroujeni, I. Filanovsky, and K. Moez, "A 28–30 GHz CMOS reflection-type phase shifter with full 360° phase shift range," *IEEE Trans. Circuits Syst. II, Exp. Briefs*, vol. 67, no. 11, pp. 2452–2456, Nov. 2020.

[15] T.-W. Li and H. Wang, "A millimeter-wave fully integrated passive reflection-type phase shifter with transformer-based multi-resonance loads for 360° phase shifting," *IEEE Trans. Circuits Syst. I, Reg. Papers*, vol. 65, no. 4, pp. 1406–1419, Apr. 2018.

[16] H. Zarei, C. T. Charles, and D. J. Allstot, "Reflective-type phase shifters for multiple-antenna transceivers," *IEEE Trans. Circuits Syst. I, Reg. Papers*, vol. 54, no. 8, pp. 1647–1656, Aug. 2007.

[17] P. Gu and D. Zhao, "Geometric analysis and systematic design of a reflective-type phase shifter with full 360° phase shift range and minimal loss variation," *IEEE Trans. Microw. Theory Techn.*, vol. 67, no. 10, pp. 4156–4166, Oct. 2019.

WENJIAN MA received the B.E. and M.E. degrees from the University of Electronic Science and Technology of China, in 2014 and 2017, respectively. He is currently an Experimentalist with the University of Electronic Science and Technology of China. His main research interests include wireless communication technology, testing technology and instruments, and intelligent anti-interference signal processing.

PEI ZOU received the B.S. and M.S. degrees from the University of Electronic Science and Technology of China, in 2014 and 2017, respectively. She is currently an Engineer with the Tenth Institute of China Electronics Technology Group Corporation. Her main research interest includes RF communication technology.

LIBING BAI (Member, IEEE) received the B.S. and Ph.D. degrees from the University of Electronic Science and Technology of China, Chengdu, China, in 2008 and 2013, respectively. He was a Visiting Research Scholar with Newcastle University, Newcastle upon Tyne, U.K. He is currently a Professor with the School of Automation Engineering, University of Electronic Science and Technology of China. His current research interests include novel sensing and precision measurement, nondestructive testing and prognostics, and health management of structure and electronic equipment.

KAI CHEN (Member, IEEE) received the B.E., M.S., and Ph.D. degrees from the University of Electronic Science and Technology of China, in 2008, 2011, and 2015, respectively. He is currently a Professor and a M.S. Supervisor with the University of Electronic Science and Technology of China. His main research interests include wireless communication technology, electronic test instruments, and equipment comprehensive tests.

• • •